Enhancing corrosion resistance of plasma electrolytic oxidation coatings on AM50 Mg alloy by inhibitor containing Ba(NO₃)₂ solutions

Jirui Ma[1], *Xiaopeng Lu*[1],✉, *Santosh Prasad Sah*[2], *Qianqian Chen*[1], *You Zhang*[3],✉, *and Fuhui Wang*[1]

1) Corrosion and Protection Center, Northeastern University, Shenyang, 110819, China
2) Faculty of Engineering, Hokkaido University, Hokkaido 060-8628, Japan
3) College of New Materials and Chemical Engineering, Beijing Institute of Petrochemical Technology, Beijing 102617, China

Abstract: To enhance the long-term corrosion resistance of the plasma electrolytic oxidation (PEO) coating on the magnesium (Mg) alloy, an inorganic salt combined with corrosion inhibitors was used for posttreatment of the coating. In this study, the corrosion performance of PEO-coated AM50 Mg was significantly improved by loading sodium lauryl sulfonate (SDS) and sodium dodecyl benzene sulfonate into Ba(NO₃)₂ post-sealing solutions. Scanning electron microscopy, X-ray photoelectron spectroscopy, X-ray diffraction, Fourier transform infrared spectrometer, and ultraviolet–visible analyses showed that the inhibitors enhanced the incorporation of BaO₂ into PEO coatings. Electrochemical impedance showed that post-sealing in Ba(NO₃)₂/SDS treatment enhanced corrosion resistance by three orders of magnitude. The total impedance value remained at 926 Ω·cm² after immersing in a 0.5wt% NaCl solution for 768 h. A salt spray test for 40 days did not show any obvious region of corrosion, proving excellent post-sealing by Ba(NO₃)₂/SDS treatment. The corrosion resistance of the coating was enhanced through the synergistic effect of BaO₂ pore sealing and SDS adsorption.

Keywords: Mg; plasma electrolytic oxidation; posttreatment; corrosion resistance

1. Introduction

Magnesium (Mg) alloy is a lightweight structural material that has attracted significant attention because of its exceptional properties; however, its application is restricted because of poor corrosion resistance [1–4]. Various treatments have been investigated to improve the corrosion performance of Mg alloy, including chemical conversion coatings, electrodeposition, anodizing, and plasma electrolytic oxidation (PEO) [5–10]. Among these techniques, PEO is a promising and environmentally friendly surface treatment method that improves the corrosion and wear resistance of Mg alloy, as well as its dielectric and thermal barrier properties. Generally, PEO coatings have a two-layer structure [11–13]. During the PEO treatment, micropores are created in the outer porous layer due to sparks and gas bubbling [14–17]. The inherent process of coating growth by spark discharge makes it almost impossible for the coating to be completely free of micropores and defects after PEO [18–20]. Despite being coated with PEO, the samples are still susceptible to corrosion [21–25].

Sealing treatment is crucial for repairing the surface defects in PEO coatings because it enhances their corrosion resistance [26–31]. Boiling water immersion is a relatively simple posttreatment method that can improve the properties of PEO coatings by producing hydroxides and oxides that partially block the pores of the coating, thereby enhancing its corrosion resistance [32]. It is also possible to enhance corrosion resistance by subjecting the coated material to various immersion treatments in different inorganic salt solutions, following the same principle. For instance, Pezzato *et al*. [33] reported the sealing of PEO coatings using a posttreatment solution containing neodymium (Nd)-sulfate salt. Electrochemical impedance spectroscopy (EIS) results demonstrate that the corrosion performance of sealed samples was significantly enhanced because of the physical barrier generated by Nd oxide deposited on the surface of the coating. Mohedano *et al*. [28,34] investigated the influence of cerium-based salt and treatment time on the sealing effect. They found that increasing the concentration of cerium salts could increase the deposited amount of cerium products to improve the barrier properties of the layer. However, prolonged treatment can lead to excessive dissolution of the original oxide coating, leading to reduced long-term corrosion resistance. Barium salt, a commonly used inorganic salt, has shown great potential in protecting metals from corrosion [35–36]. Liu *et al*. [37] produced barium phosphate coatings on AZ91 Mg alloy, which exhibited better corrosion resistance than manganese phosphate conversion film. Chen *et al*. [38] also obtained barium conversion films on AZ31 alloy, which increased the corrosion resistance by about one order of magnitude. Although barium salts have been extensively studied

Springer

for producing conversion films, there has been no research on the use of barium salt solutions to seal the pores of PEO coatings.

The amount of deposition on the sample surface during immersion usually depends on the concentration of inorganic salts in posttreatment solution and the duration of the posttreatment. However, increasing both factors may result in excessive coating erosion owing to the posttreatment solution. To optimize the deposition amount, the coating can be modified with an anionic corrosion inhibitor. Anionic surfactants have been reported to complex heavy metal cations in wastewater as anionic surfactants [39–41]. Sodium dodecyl benzene sulfonate (SDBS) and sodium lauryl sulfonate (SDS) are excellent corrosion inhibitors for Mg alloys [42–46]. Frignani *et al*. [47] reported the corrosion inhibition of anionic surfactants in electrolyte solution for Mg alloy. They found that the inhibitor adsorbs quickly on the Mg surface and limits the cathodic reaction while reacting with Mg^{2+} to form a precipitation layer. Li *et al*. [48] proposed that SDS could form a protective corrosion layer by chemically bonding with AlMn intermetallic on the Mg surface during immersion in NaCl solution. The inhibitor effectively inhibits Mg alloy corrosion through physical and chemical adsorption, thereby preventing microgalvanic corrosion. In this study, we developed a novel sealing posttreatment technology for AM50 Mg alloy using a Ba-based environmental PEO coating. Anionic inhibitors, SDS and SDBS, are effective surface modifiers and efficient corrosion inhibitors for Mg alloys. As the dissolution/precipitation reaction during sealing is of great importance to the final corrosion properties of the coating, we examined the changes in the morphology and composition of PEO coating in the presence of different inhibitors. We also investigated the corrosion properties of the PEO-treated samples after performing sealing treatment.

2. Experimental

2.1. Materials and coating preparation process

In this study, we used the AM50 Mg alloy, the composition of which could be found in a previously published paper [49]. Before PEO treatment, the specimens with dimensions of 20 mm × 20 mm × 6 mm were ground using SiC abrasive papers lubricated with water in a sequence ranging from #80 to #1000 grit and finally air-dried. The treatment was conducted with a pulsed DC (Direct current) power supply operating in a constant current mode and was further treated in a constant voltage mode of 450 V for 13 min. The duty ratio and frequency were 30% and 500 Hz, respectively. During

the PEO treatment, the anode and cathode were made of the Mg alloy sample and carbon plate, respectively. The electrolyte comprised Na_2SiO_3 (30 g·L^{-1}), KF (8 g·L^{-1}), and NaOH (4 g·L^{-1}) in distilled water. A cooling system was used to maintain the temperature of the PEO electrolytes at (25 ± 3)°C.

After the PEO treatment, the sample was subjected to a sealing treatment by immersing it in an aqueous solution containing Ba-salts for 1 h at 50°C. The posttreatment solution comprised 20g·L^{-1} $Ba(NO_3)_2$ and 10 g·L^{-1} H_2O_2, with pH adjusted to 4 by adding diluted nitric acid. To examine the influence of anionic surfactants, 0.1 mol·L^{-1} SDS and SDBS were added to the sealing electrolyte, and the solution was stirred in a magnetic heating agitator to ensure uniformity. After the sealing treatment, the samples were rinsed with deionized water and dried with compressed air. The coatings were labeled as follows: PEO coating (blank PEO coating), PEO–Ba coating (PEO coating treated with barium nitrate solution only), PEO–Ba–SDS coating (PEO coating treated with barium nitrate solution and SDS), and PEO–Ba–SDBS coating (PEO coating treated with barium nitrate solution and SDBS), to indicate the composition of the different posttreatment solutions.

2.2. Microstructure and composition of the coatings

The scanning electron microscope (SEM, Quanta250FEG, FEI Company, Czech) equipped with an energy dispersive spectrometer (EDS) system was used to obtain the surface and cross-section morphology of the coatings. The composition of the coating elements is shown in Table 1. The phase composition of the coating was analyzed using X-ray diffraction (XRD, Smartlab, Rigaku, Japan) with a grazing angle of 0.5° and a 2θ range of 20°–80°. X-ray photoelectron spectroscopy (XPS, Model Axis Supra, Shimazu-Kratos Analytical, UK) was also used to analyze the phase composition of the coating in depth. Fourier transform infrared spectrometer (FTIR, Thermo Fisher, USA) was used to investigate chemical bonds in the coating from 600 to 4000 cm^{-1}. An Ultraviolet–visible spectrophotometer (Thermo Fisher, USA) was used for UV–Vis spectral measurements. The samples loaded with corrosion inhibitors were immersed in 0.5wt% NaCl solutions to prepare solutions for different immersion periods. The absorption spectra of these solutions were determined with the 0.5wt% NaCl solution as a reference.

2.3. Corrosion measurements

A three-electrode cell was used to examine the electrochemical properties of corrosion. The cell comprised the same sample as the working electrode, a saturated calomel

Table 1.   EDS area analysis of the studied specimens   at%

Treatment	Mg	O	Na	Al	Si	Ba
PEO	33.1	38.0	2.3	2.3	24.3	
PEO–Ba	29.1	37.0	1.1	3.2	21.0	0.8
PEO–Ba–SDS	25.0	37.0	0.9	1.9	17.3	17.9
PEO–Ba–SDBS	29.2	42.4	2.1	2.0	18.7	5.7

electrode as the reference electrode, and a platinum plate as the counter electrode. EIS was conducted using the electro-chemical workstation (Versa STAT 3F, Ametek, USA) at open circuit potential with a 10 mV RMS (Root mean square) sinusoidal perturbation over a scanning frequency range of 10^{-2}–10^5 Hz with 36 points for the full frequency range. The experiments were conducted in a 0.5wt% NaCl solution. The impedance spectra were analyzed using the ZSimpWin soft-ware. All the experiments were repeated more than thrice to confirm the reproducibility of the remarkable features of the spectra. In the spectra, markers are observed data points, and lines are the fitting data.

To estimate the corrosion resistance of the coating, a salt spray test was conducted following the ASTM B117 cri-terion. The test was conducted by creating a salt spray atmo-sphere using an aqueous solution of 5wt% NaCl at a neutral pH and a temperature of 35°C. Three samples were prepared for each sample to ensure repeatability. After testing, the sur-face corrosion was observed by photographing the macro-morphology of the coating using a digital camera.

3. Results and discussion

3.1. Microstructure and composition of the coatings

The surface micrographs of the unsealed and sealed coat-ings (Fig. 1) revealed distinct differences among different posttreatment solutions. The coating surface (Fig. 1(a)) was dominated by many pores, which is a typical characteristic of PEO-coated Mg. The coating surface sealed with the barium salt solution had no significant deposits, and the morphology was similar to that of the unsealed PEO coating. However, after the addition of SDS or SDBS, many deposits were ob-served on the coating surface (Fig. 1(c) and (d)). The effect of surfactants was clearly reflected in the surface morphology of the coating, as they contributed significantly to the deposited products. The number of open pores in the coating was re-duced after the posttreatment because of the accumulation of deposits in the pores. Bayram *et al.* [50] found that surfactant results in the surface potential being negative due to adsorp-tion on the surface. Therefore, the addition of SDS and SDBS
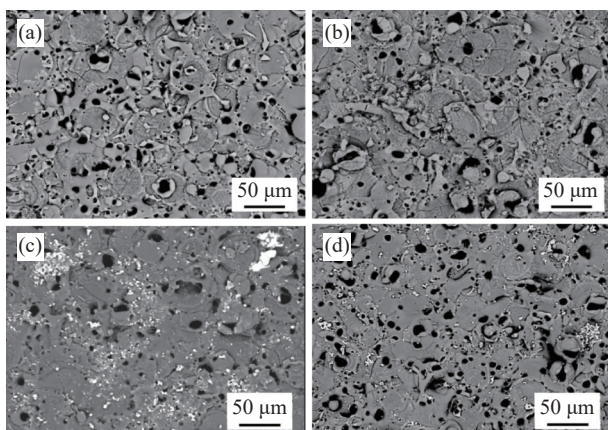
leads to a negative change in the coating surface potential. This may be the main reason for the increased surface depos-ition on the coating with the addition of both surfactants. Table 1 shows the chemical composition of the samples. The coating mainly consisted of Mg, Si, and O. Remarkably, the addition of corrosion inhibitors significantly increased bari-um content (~18at%), especially when SDS was added to the solution. Research has shown that the hydrophilic–lipophilic balance of SDS was higher than that of SDBS, and the wet-ting time was shorter than that of SDBS [51]. This suggests that the presence of SDS in the electrolyte easily decreases the surface tension of the coating compared with SDBS, res-ulting in more deposition on the PEO coating.

Fig. 2 shows the cross-section microstructure of the samples. The figure shows that the coating was relatively uniform (approximately 30 μm), which could be divided into two layers, and discharge channels were evident throughout the layers. Comparing the cross-sectional morphologies of the samples after the sealing treatments, it was apparent that the coatings sealed with only barium salts were the most por-ous and defective. This is most likely because of the acidic sealing electrolyte, which corrodes the original oxide coating (Fig. 2(b)). Moreover, no significant deposits were detected in the pores of the coatings. The surfaces of the samples sealed with surfactants exhibited a thin layer of deposition that adhered to the outer layer, obstructing the discharge channels of the coating.
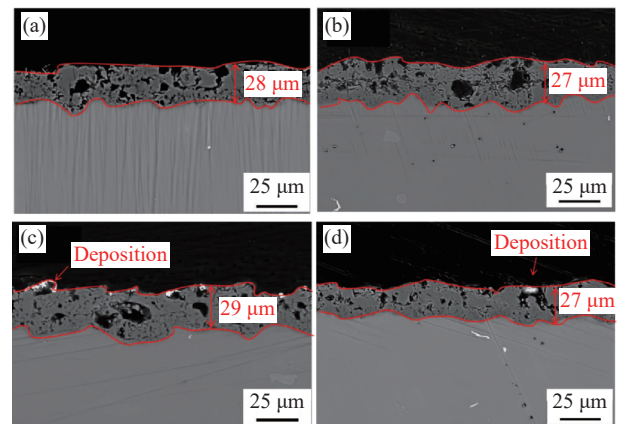

Fig. 2.   Cross-sectional micrographs of PEO-coated Mg alloy before and after posttreatment in different electrolytes: (a) PEO; (b) PEO–Ba; (c) PEO–Ba–SDS; (d) PEO–Ba–SDBS.

The SEM and EDS maps (Mg, O, Si, and Ba elements) of the different coatings revealed noticeable morphological and microstructural distinctions on the surfaces and cross-sec-tions (Figs. 3–5). From the EDS mapping, only a minor amount of Ba was present on the outer layer of the PEO–Ba coating (Fig. 3). However, the addition of surfactants to the sealing solution resulted in a significant accumulation of Ba-containing product that deposited into large-sized defects in the coating (Figs. 4 and 5). The PEO–Ba–SDS coating had the most obvious difference in that depositions were present in almost every micropore. The EDS results (Table 1) showed that the Ba content in the PEO–Ba–SDS coating de-
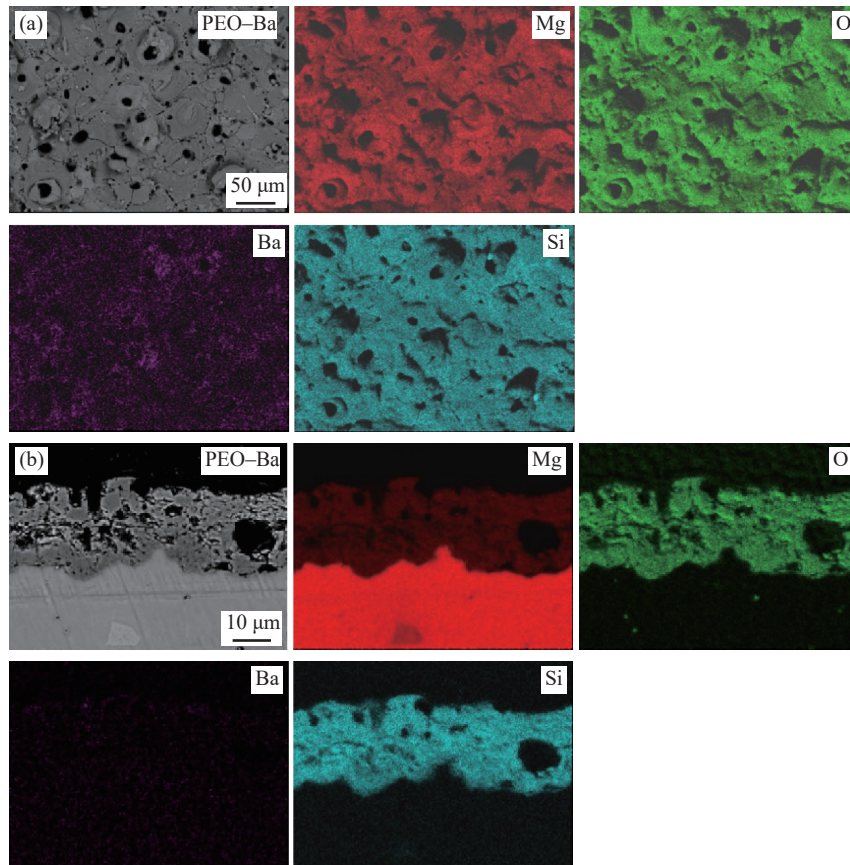

Fig. 1.   Surface micrographs of PEO coatings before and after posttreatment in different electrolytes: (a) PEO; (b) PEO–Ba; (c) PEO–Ba–SDS; (d) PEO–Ba–SDBS.

Fig. 3.   EDS maps of the PEO coatings after posttreatment in Ba(NO$_3$)$_2$ electrolytes: (a) surface micrograph; (b) cross-sectional micrograph.
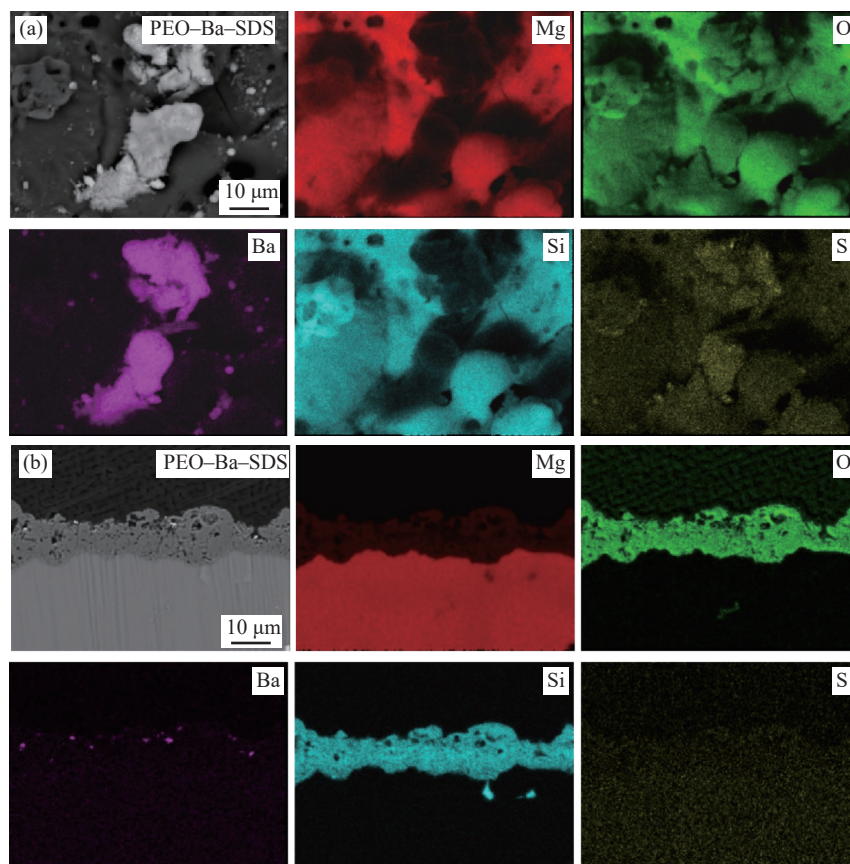

Fig. 4.   EDS maps of the PEO coatings after posttreatment in Ba(NO$_3$)$_2$ + 0.1 mol·L^{-1} SDS electrolytes: (a) surface micrograph; (b) cross-sectional micrograph.
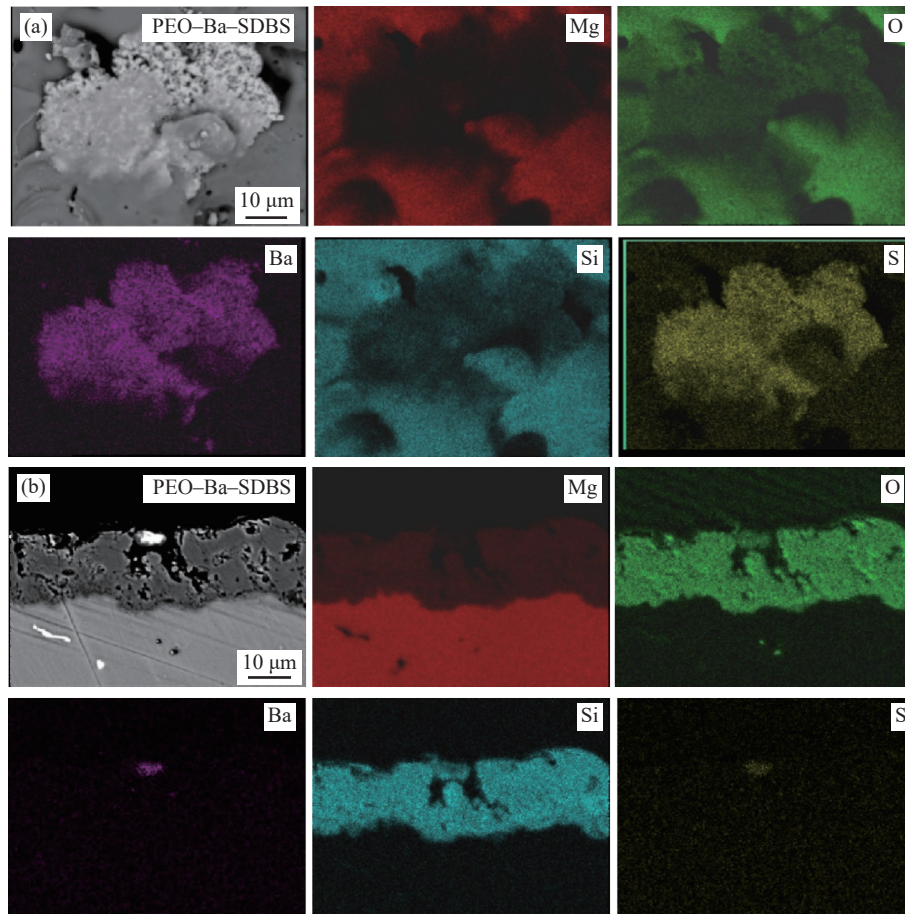
Fig. 5.   EDS maps of the PEO coatings after posttreatment in Ba(NO₃)₂ + 0.1 mol·L⁻¹ SDBS electrolytes: (a) surface micrograph; (b) cross-sectional micrograph.

position layer was 17.9at%, and the Ba content in the PEO–Ba–SDBS coating was 5.7at%.

The XRD analysis showed that the coating formed on the AM50 alloy in the silicate-based electrolyte mainly consisted of two crystalline phases, MgO and Mg₂SiO₄ (Fig. 6). The Mg peaks were also detected because of the porous structure of the coating. The posttreatment coating did not form any new Ba-containing phase because of the low Ba-containing products in the coating.

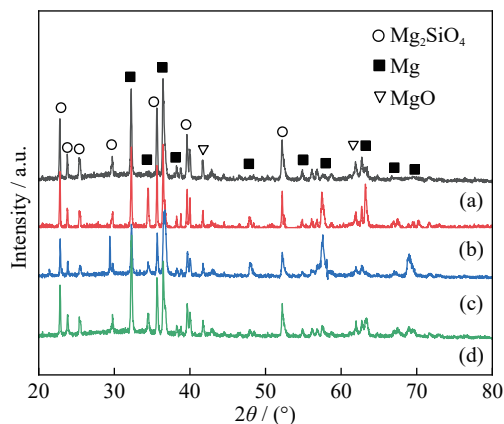Fig. 7 shows the XPS and high-resolution spectra (Ba 3d,

Fig. 6.   XRD patterns of different coatings: (a) PEO; (b) PEO–Ba; (c) PEO–Ba–SDS; (d) PEO–Ba–SDBS.

S 2p, and Mg 1s) of the posttreated samples. In the Ba 3d spectra of posttreated samples, two distinctive peaks correspond to Ba 3d 3/2 at a lower energy of 780.2 eV and Ba 3d 1/2 at a higher energy with a separation of approximately 14.9 eV, corresponding to Ba^{2+} in the formation of BaO_2 and $Ba(OH)_2$ (Fig. 7(b) and (f)). The Mg 1s spectrum was fitted with peaks at 1304.2 eV, corresponding to MgO (Fig. 7(c) and (g)). The S 2p spectra showed peaks at 178.4 and 168.2 eV, corresponding to SO_4^{2-} and SO_3^{2-} (Fig. 7(d) and (h)) because of the adsorbed SDS and SDBS on the surface of the coating, respectively (Fig. 7(e) and (f)).

With the addition of surfactants to the posttreatment solution, it was adsorbed to the surface of the coating, which triggered a reaction between Ba^{2+} carried by the inhibitor and OH^- on the surface of the coating, as shown in Eq. (1). The pH of the SDS-containing solution increased from 8.4 to 8.6, and that of the SDBS-containing solution increased from 7.9 to 8.2. The change in pH can be attributed to the hydrolysis of the corrosion inhibitors, where the sulfonic and benzene sulfonic groups react with hydrogen ions in the solution. The reaction of H_2O_2 in the sealing solution with the deposited $Ba(OH)_2$ resulted in the formation of BaO_2 on the sample surface. The overall reaction formulas for the process are given in Eq. (2):

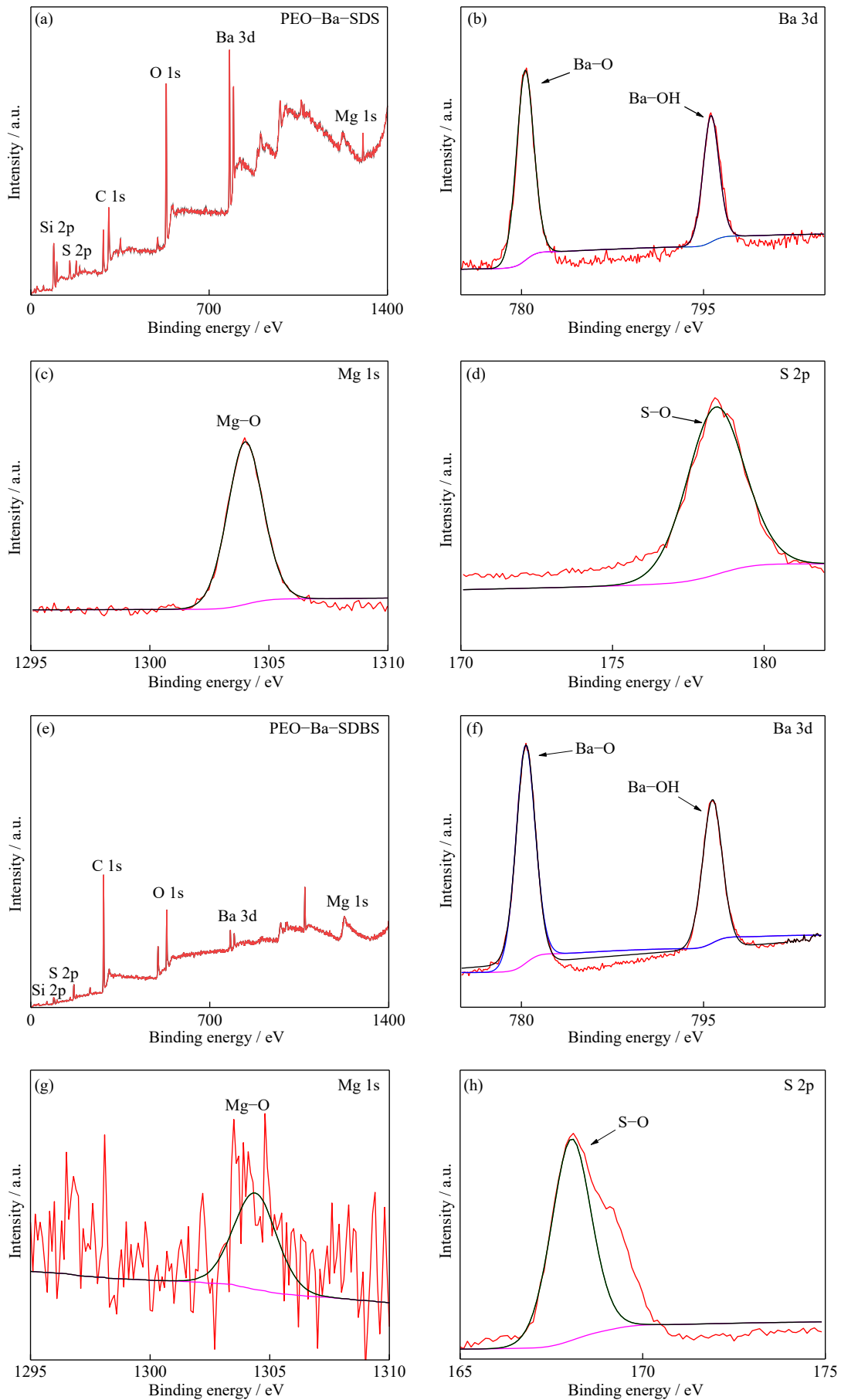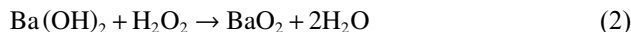$$Ba^{2+} + 2OH^- \rightarrow Ba(OH)_2(s) \tag{1}$$
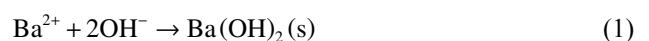
Fig. 7. XPS results of PEO–Ba–SDS coating: (a) survey spectra, (b) Ba 3d, (c) Mg 1s, and (d) S 2p; XPS results of PEO–Ba–SDBS coating: (e) survey spectra, (f) Ba 3d, (g) Mg 1s, and (h) S 2p.

$$Ba(OH)_2 + H_2O_2 \rightarrow BaO_2 + 2H_2O \qquad (2)$$

Based on the data found in *Lange's Handbook of Chemistry* [52], the standard enthalpy of formation (ΔH) and standard entropy of formation (ΔS) of the substances in Eq. (2) can be determined. Specifically, $Ba(OH)_2$ has a ΔH of -986.2 kJ·mol^{-1} and a ΔS of 132.4 J·mol^{-1}·K^{-1}. H_2O_2 has a ΔH of -187.8 kJ·mol^{-1} and a ΔS of 110.5 J·mol^{-1}·K^{-1}. BaO_2 has a ΔH of -619.0 kJ·mol^{-1} and a ΔS of 120.2 J·mol^{-1}·K^{-1}. H_2O has a ΔH of -285.83 kJ·mol^{-1} and a ΔS of 69.91 J·mol^{-1}·K^{-1}. Using Eq. (3), which introduces the thermodynamic temperature (T) value, we obtained a standard molar Gibbs free energy (ΔG) <0, indicating that the reaction can proceed.

$$\Delta G = \Delta H - T\Delta S \qquad (3)$$

The influence of surfactants on the two coatings was also supported by the FTIR spectra (Fig. 8). The adsorption peak at 860 cm^{-1} showed the symmetric stretching vibration of Si–O–Si, confirming the existence of Mg_2SiO_4 in the PEO coating. Meanwhile, the Mg–O peak at 506 cm^{-1} confirmed the formation of MgO [53]. The weak broadband appearing at 1120–1180 cm^{-1} demonstrated the vibrational band of the sulphonate group. The sulfate S=O stretching vibrational band at 1204 cm^{-1} indicates v(S=O) symmetric vibrations, where v denotes the stretching vibration. This confirmed the adsorption of SDBS and SDS on the surface of the coating [54]. The absorption peak of the barium salt failed to appear, which might be due to the low BaO_2 content of the coating surface.
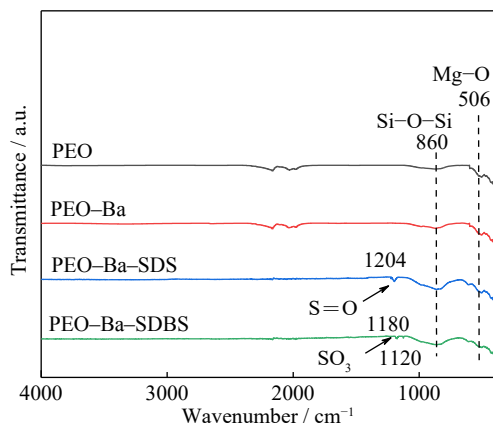

Fig. 8.   FTIR spectra of the two coatings with added corrosion inhibitors.

3.2. Corrosion performance

Fig. 9 shows the corrosion behavior of the different samples observed with EIS measurement. In the Bode diagram, the line is the fitting data, whereas in the phase diagram, the transition between peaks and valleys implies the occurrence of one time constant. The initial increase in low-frequency impedance and further changes indicate that the discharge channels are initially sealed/filled with corrosion products, and such a process is marked with a new time constant. The corrosion products formed on the PEO and

PEO–Ba coatings or PEO–Ba–SDS or PEO–Ba–SDBS coatings should be different, and they were observed with a higher frequency time constant (Fig. 9). The chemical stability and morphology of corrosion products determine the suppression or enhancement of corrosion. The difference and evolution of the corrosion behavior of the coatings are represented by equivalent circuits and parameters (Fig. 10(a) and Table 2). R_c and CPE_c represent the values of the resistance of the porous coating and its capacitance, respectively. R_{ct} represents the charge transfer resistance value of these samples, and CPE_{dl} represents the double-layer capacitance value at the electrolyte/metal interface. The n (n_1, n_2) is an index ranging from 0 to 1 and it affect the converting of CPE_c or CPE_{dl} into resistance (n_1 or $n_2 = 0$) or capacitance (n_1 or $n_2 = 1$). λ^2 is the fitted quality parameter. A bit higher error was observed in the fitting data (λ^2, Table 2), which could be attributed to the complicated response from the complicated microstructure of the coatings. In the bare PEO-coated sample, the low-frequency (f) impedance ($|Z|_{f=0.01 \text{ Hz}}$) reached its highest value at 96 h of immersion, about 230 kΩ·cm^2, which others decreased. The highest impedance is attributed to sealing pores with corrosion products, whose formation is mostly reflected in the second time constant. The disappearance of the high-frequency time constant (in the range of 10^3–10^5 Hz) was attributed to the accelerated loss of the protective ability of the coating (Fig. 9(a)). The corrosion products formed on the PEO–Ba coating are marked with a time constant of higher frequency (Fig. 9(b)). Although the corrosion products are relatively more protective initially, corrosion is accelerated. This can be attributed to the excessive corrosion of the interior of the coating by the posttreatment solution. PEO–Ba–SDS or PEO–Ba–SDBS coatings are rather highly corrosion resistant in a 0.5wt% NaCl solution. The stability of corrosion products formed on PEO–Ba–SDS is better than that on PEO–Ba–SDBS coating. The inverse of R_{ct} plotted with time reflects the evolution of corrosion during immersion in NaCl solution (Fig. 10(b)).

Although PEO–Ba coating showed better resistance to corrosion than PEO initially, it suffered badly upon extended immersion (>100 h). PEO–Ba–SDS and PEO–Ba–SDBS coatings were resistant to corrosion, and PEO–Ba–SDS coating showed the lowest corrosion rate for 768 h with the R_{ct} of 926 kΩ·cm^2 (Table 2). It can be inferred that the inhibitor was integrated into the coating, which altered its microstructure and composition, resulting in enhanced impedance at the initial stage of the corrosion test. These results showed the coating pretreated with $Ba(NO_3)_2$/inhibitors provided more effective corrosion protection than the bare PEO coating. BaO_2 was deposited in open pores by pretreatment to enhance corrosion resistance, as observed from the high impedance of PEO–Ba–SDS and PEO–Ba–SDBS coatings. Corrosion inhibition and pores sealing are responsible for the enhanced corrosion resistance. BaO_2 deposited in the pore of the coating is likely subjected to slow hydrolysis to form a
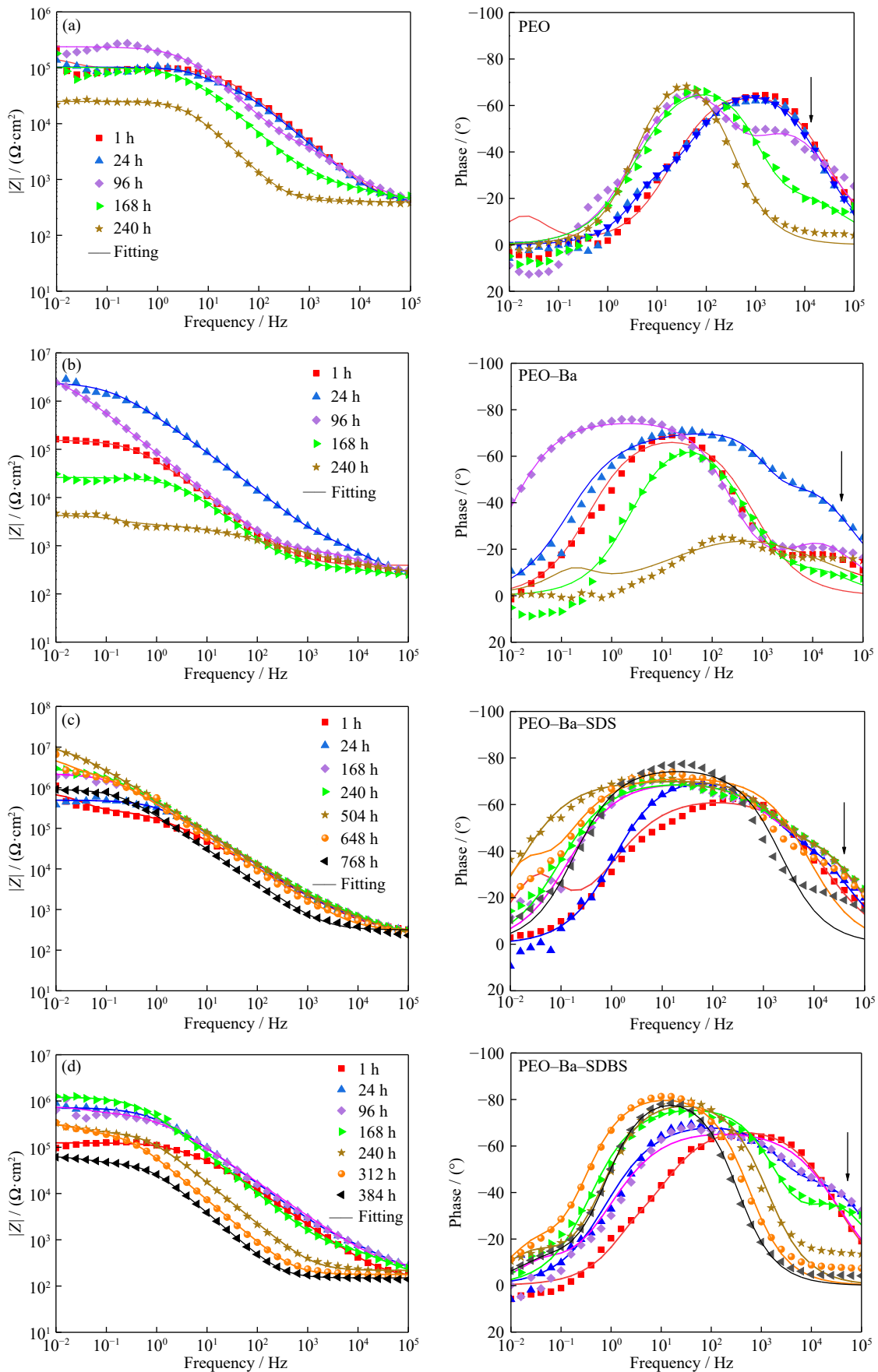
Fig. 9. Evaluation of corrosion resistance of (a) PEO, (b) PEO–Ba, (c) PEO–Ba–SDS, and (d) PEO–Ba–SDBS coating during immersion in 0.5wt% NaCl solution.
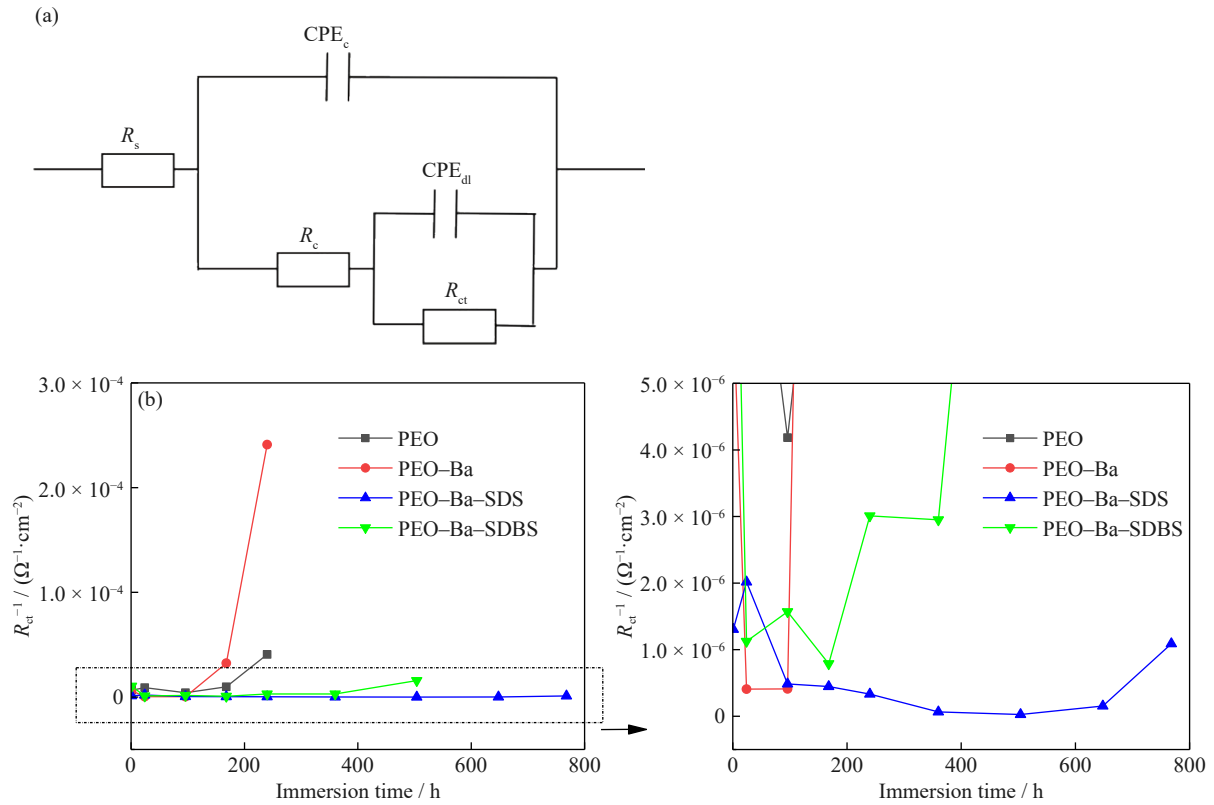
Fig. 10. (a) Equivalent circuit used for fitting the observed data and (b) evolution of corrosion resistance in 0.5wt% NaCl solution at 25ºC.

Table 2. Fitting results for the impedance spectra of Fig. 9.

Treatment	Time / h	R_c / (k$\Omega \cdot$ cm^2)	CPE$_c$ / (μF$\cdot$s^{-n} $\cdot$ cm^{-2})	n_1	R_{ct} / (k$\Omega \cdot$ cm^2)	CPE$_{dl}$ / (μF$\cdot$s^{-n} $\cdot$ cm^{-2})	n_2	λ^2 / 10^{-3}
PEO	1	58.54	0.23	0.8	64.60	1.80	0.9	3.7
	24	69.08	0.23	0.8	39.59	0.91	0.9	1.6
	96	8.40	0.31	0.7	230.6	0.97	0.9	1.5
	168	0.55	0.27	0.8	88.78	0.49	0.8	3.9
	240	0.42	2.4	0.9	24.12	1.49	0.9	8.5
PEO–Ba	1	0.46	2.21	0.7	156.59	1.30	0.9	1.9
	24	0.58	0.17	0.8	3937.90	1.90	0.9	2.5
	96	0.63	0.66	0.7	4082.60	1.90	0.9	2.6
	168	0.14	0.84	0.8	28.73	1.34	0.8	1.2
	240	0.45	4.88	0.5	1.89	8.30	0.7	0.7
PEO–Ba–SDS	1	105.60	0.55	0.8	985.20	2.30	0.9	13.0
	24	53.15	0.53	0.8	555.80	4.75	0.8	11.0
	168	1.93	0.24	0.8	2224.90	0.26	0.8	7.4
	240	1.66	0.22	0.8	29995.90	0.29	0.8	4.7
	504	0.88	0.91	0.9	126.53	0.41	0.8	2.9
	648	0.96	0.19	0.8	2475.70	0.31	0.9	10.2
	768	0.48	0.66	0.8	926.22	0.31	1	6.6
PEO–Ba–SDBS	1	103.54	0.56	0.8	32.11	2.60	1	0.3
	24	1.17	0.13	0.8	660.36	0.25	0.8	4.3
	96	1.41	0.16	0.8	517.60	0.21	0.8	4.6
	168	0.79	0.21	0.8	1206.70	0.19	0.9	13.2
	240	0.87	1.60	0.9	256.30	0.25	0.7	50.1
	312	0.64	3.40	0.9	252.21	1.72	0.7	35.3
	384	0.61	6.10	0.9	53.01	8.7	0.8	24.3

protective Ba(OH)$_2$ layer, and at the same time, corrosion inhibitor inhibits corrosion. However, the inner layer penetrated for a prolonged time, and the inhibitor was consumed/released, leading to corrosion at the interface between the coating and matrix. The combined presence of the inhibitor SDS and barium salt enhanced the corrosion properties of the sample. By observing the region of 10^3–10^5 Hz in the phase angle plot of Fig. 9(c) and (d), the high-frequency time constant of the PEO–Ba–SDS coating disappeared after 768 h of immersion, whereas that of the PEO–Ba–SDBS coating disappeared after 240 h of immersion. This can be attributed to the amount of deposition on the surfaces of both coatings. The coatings with SDS and SDBS also showed a maximum phase angle close to −80°, indicating their superior performance compared to the PEO and PEO–Ba coatings (Fig. 9(c) and (d)).

Relative differences in corrosion inhibition between SDS and SDBS were also observed in the UV–Vis absorption spectra (Fig. 11). Corrosion of the Mg alloy led to an increase in local pH value with the appearance of local pitting. The gradually released inhibitor induced the formation of a local dense protective film that blocked further expansion of the pitting corrosion. The solution immersed with the two

coatings showed strong absorption bands at 288 and 203 nm. A greater release of corrosion inhibitor and a faster release rate indicated that the coating was more susceptible to corrosion, and the PEO–Ba–SDBS coating started to release large amounts of corrosion inhibitor at the beginning of the immersion, with a rapid increase in its peak absorbance. During the entire immersion process, the corrosion inhibitor of the PEO–Ba–SDS coating was released steadily, indicating that the PEO–Ba–SDS coating exhibited better corrosion resistance. The combined effect of Ba(NO$_3$)$_2$/inhibitor pretreatment was observed after a salt spray test for 40 d. Fig. 12 shows the surface appearance of the samples. The results showed that the PEO–Ba coating experienced corrosion after immersion for 10 d, and pitting was observed on the coating surface after testing for 20 d. Compared with the PEO–Ba coating, the PEO coating exhibited a better corrosion performance with fewer corroded areas. A few corrosion pits appeared in the PEO–Ba–SDS coating after 40 d of immersion, whereas the PEO–Ba–SDS coating exhibited superior corrosion performance with no visible corrosion pits. These results suggested that SDS and SDBS remarkably enhance the corrosion resistance of the PEO–Ba coating.
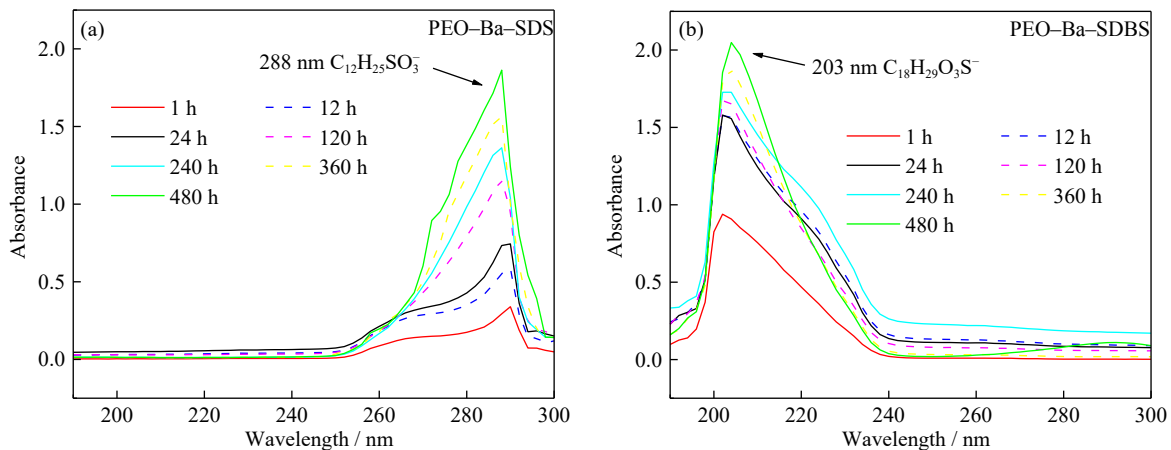

Fig. 11. UV-vis absorption spectra of inhibitor in coating: (a) PEO–Ba–SDS; (b) PEO–Ba–SDBS.

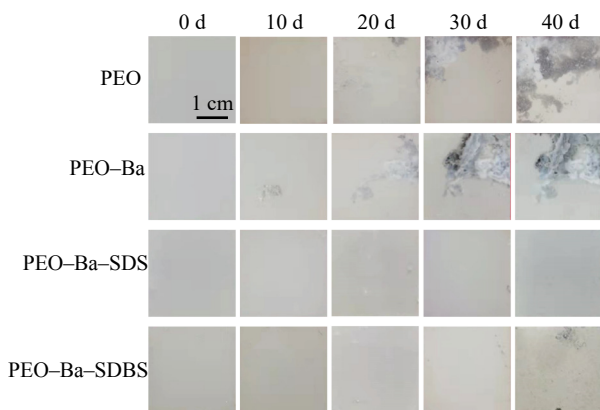Figs. 13 and 14 show the surface morphologies of

Fig. 12. Surface appearance of the PEO coatings and sealing before and after salt fog corrosion test.

PEO–Ba–SDS and PEO–Ba–SDBS coatings after testing for 240 h in NaCl solution. Interestingly, the BaO$_2$ particles grew significantly from 5–10 μm to 25–50 μm because of the corrosion. This growth of BaO$_2$ particles was attributed to the increased corrosion resistance (Figs. 9 and 10) during immersion. The growth of BaO$_2$ particles can seal the pores of the PEO–Ba–SDS or PEO–Ba–SDBS coatings. However, because the granular microstructure of BaO$_2$ pores is not perfectly sealed, corrosion inhibitors play a crucial role in enhancing corrosion resistance (Fig. 15). Considering the microstructure of the sample, the inhibitor molecules were substantially adsorbed on the surface of the coating during the initial stage of the posttreatment process. SDS and SDBS adsorption leads to negative changes in surface potentials. The positively charged barium ions released during hydrolysis interact with the negatively charged regions, creating an elec-
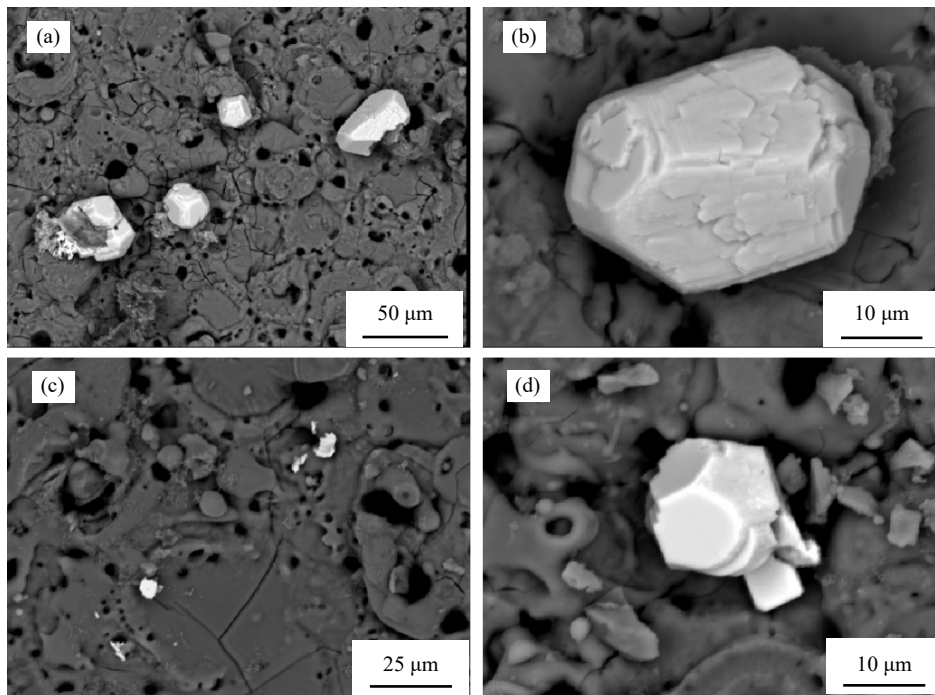
Fig. 13.   Surface micrographs of different coatings after immersion for 240 h in 0.5wt% NaCl solution: (a, b) PEO–Ba–SDS; (c, d) PEO–Ba–SDBS.
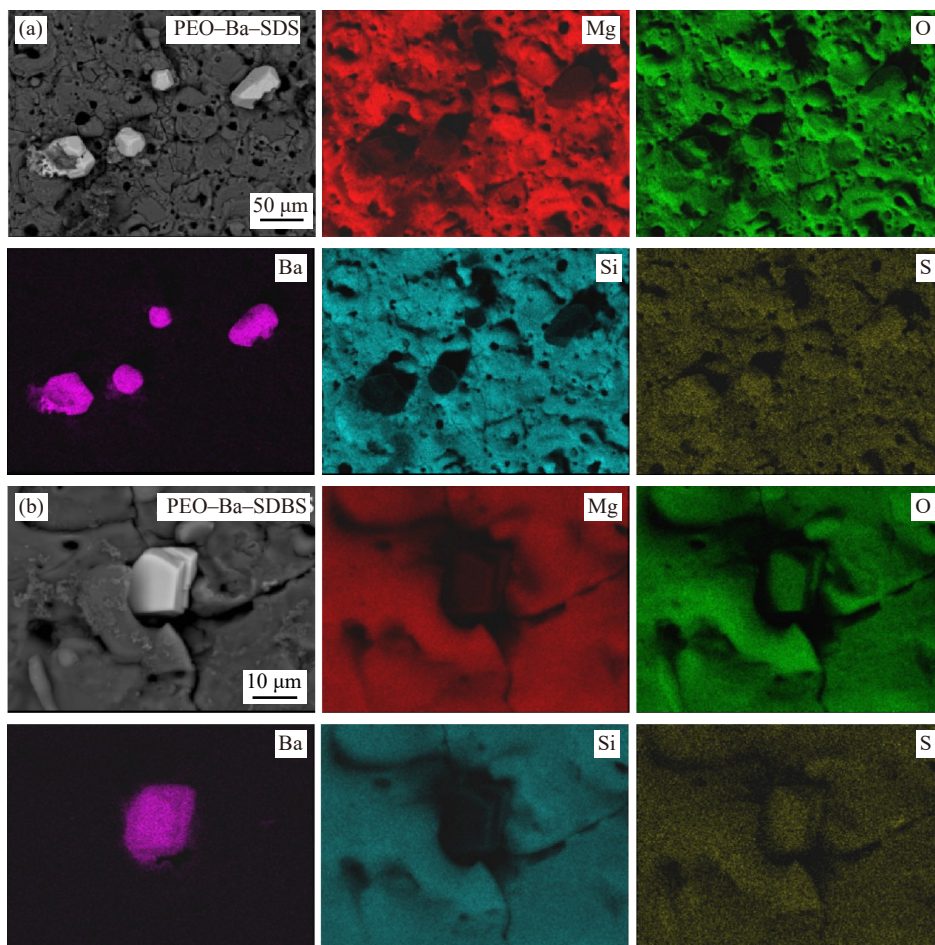

Fig. 14.   EDS maps of the coatings after immersion for 240 h in 0.5wt% NaCl solution: (a) PEO–Ba–SDS; (b) PEO–Ba–SDBS.

trostatic attraction between them (Fig. 15). The reaction of barium ions on the coating surface increased the amount of

deposited product. During the early stage of immersion, the coating primarily blocked the invasion of the corrosion me-
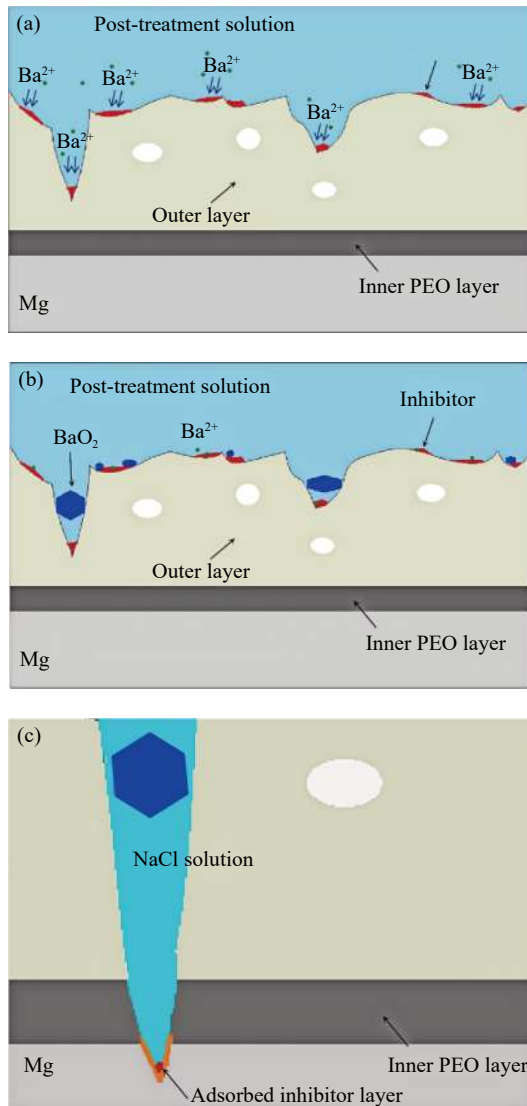
Fig. 15. **Schematic illustration of the corrosion protection mechanism of the posttreatment coating: (a) diagram of the initial stage of posttreatment; (b) diagram of the completed posttreatment; (c) active protection mechanisms for incorporated inhibitor.**

dia, and the coating surface adsorption of corrosion inhibitors also provided protection. As the immersion time increased, the corrosion inhibitor stored inside the coating began to be released, forming a dense protective film that inhibited local corrosion.

4. Conclusions

(1) In this study, we developed a sealing posttreatment for AM50 Mg coated with PEO and corrosion inhibitors. The sealing process significantly improved the corrosion performance of the coating. The introduction of SDS to the sealing solution resulted in protective deposition products on the PEO coating surface.

(2) BaO_2 was the predominant component of the deposition layer. We demonstrated that the corrosion inhibitor was effectively loaded into the interior of the coating and was continuously released to protect the coating during immer-

sion.

(3) The corrosion inhibitors and inorganic salts used in the sealing treatment significantly improved the corrosion performance of the coating. The impedance of the SDS-containing coating was maintained at 926 $\Omega \cdot cm^2$ after 768 h of immersion in 0.5wt% NaCl solution, and the coating showed no signs of corrosion after 40 d of salt spray test.

Acknowledgements

Conflict of Interest

All authors do not have competing interests to declare.

References

[1]   J.J. Wang, K.X. Zhang, G.B. Ying, *et al.*, Effects of RE (RE = Sc, Y and Nd) concentration on galvanic corrosion of Mg–Alloy: A theoretical insight from work function and surface energy, *J. Mater. Res. Technol.*, 24(2023), p. 6958.

[2]   D.D. Zhang, F. Peng, and X.Y. Liu, Protection of magnesium alloys: from physical barrier coating to smart self-healing coating, *J. Alloys Compd.*, 853(2021), art. No. 157010.

[3]   J.F. Song, J. She, D.L. Chen, and F.S. Pan, Latest research advances on magnesium and magnesium alloys worldwide, *J. Magnesium Alloys*, (2020), No. 1, p. 1.

[4]   M.C.L. de Oliveira, R.M.P. da Silva, R.M. Souto, and R.A. Antunes, Investigating local corrosion processes of magnesium alloys with scanning probe electrochemical techniques: A review, *J. Magnesium Alloys*, 10(2022), No. 11, p. 2997.

[5]   J.H. Liu, Z.H. Yang, D. Li, M. Li, and F.P. Bai, Resistance coefficient for large-scale roughness with seepage through porous bed, *J. Hydrol.*, 590(2020), art. No. 125498.

[6]   Y.M. Zhang, N. Li, N. Ling, J.L. Zhang, and L. Wang, Enhanced long-term corrosion resistance of Mg alloys by superhydrophobic and self-healing composite coating, *Chem. Eng. J.*, 449(2022), art. No. 137778.

[7]   L.Y. Chai, X. Yu, Z.H. Yang, Y.Y. Wang, and M. Okido, Anodizing of magnesium alloy AZ31 in alkaline solutions with silicate under continuous sparking, *Corros. Sci.*, 50(2008), No. 12, p. 3274.

[8]   M. Daavari, M. Atapour, M. Mohedano, R. Arrabal, E. Matykina, and A. Taherizadeh, Biotribology and biocorrosion of MWCNTs-reinforced PEO coating on AZ31B Mg alloy, *Surf. Interfaces*, 22(2021), art. No. 100850.

[9]   D. Saran, A. Kumar, S. Bathula, D. Klaumünzer, and K.K. Sahu, Review on the phosphate-based conversion coatings of magnesium and its alloys, *Int. J. Miner. Metall. Mater.*, 29(2022), No. 7, p. 1435.

[10] S.Y. Jin, X.C. Ma, R.Z. Wu, *et al.*, Effect of carbonate additive on the microstructure and corrosion resistance of plasma electrolytic oxidation coating on Mg–9Li–3Al alloy, *Int. J. Miner. Metall. Mater.*, 29(2022), No. 7, p. 1453.

[11] M. Molaei, K. Babaei, and A. Fattah-alhosseini, Improving the

2060

Int. J. Miner. Metall. Mater., Vol. 31, No. 9, Sep. 2024

wear resistance of plasma electrolytic oxidation (PEO) coatings applied on Mg and its alloys under the addition of nano- and micro-sized additives into the electrolytes: A review, *J. Magnesium Alloys*, 9(2021), No. 4, p. 1164.

[12] R.O. Hussein, X. Nie, and D.O. Northwood, An investigation of ceramic coating growth mechanisms in plasma electrolytic oxidation (PEO) processing, *Electrochim. Acta*, 112(2013), p. 111.

[13] W.H. Yao, L. Wu, J.F. Wang, *et al.*, Micro-arc oxidation of magnesium alloys: A review, *J. Mater. Sci. Technol.*, 118(2022), p. 158.

[14] H.Y. Fan, N. Ling, R. Bai, J.L. Zhang, and L. Wang, Influence of V-containing species on formation and corrosion resistance of PEO coatings developed on AZ31B Mg alloy, *Ceram. Int.*, 49(2023), No. 15, p. 24783.

[15] M. Molaei, A. Fattah-alhosseini, M. Nouri, P. Mahmoodi, and A. Nourian, Incorporating TiO_2 nanoparticles to enhance corrosion resistance, cytocompatibility, and antibacterial properties of PEO ceramic coatings on titanium, *Ceram. Int.*, 48(2022), No. 14, p. 21005.

[16] L. Liu, S.R. Yu, G. Zhu, *et al.*, Corrosion and wear resistance of micro-arc oxidation coating on glass microsphere reinforced Mg alloy composite, *J. Mater. Sci.*, 56(2021), No. 27, p. 15379.

[17] D. Wang, C. Ma, J.Y. Liu, *et al.*, Corrosion resistance and anti-soiling performance of micro-arc oxidation/graphene oxide/stearic acid superhydrophobic composite coating on magnesium alloys, *Int. J. Miner. Metall. Mater.*, 30(2023), No. 6, p. 1128.

[18] A.N. Buling and J. Zerrer, Increasing the application fields of magnesium by ultraceramic®: Corrosion and wear protection by plasma electrolytical oxidation (PEO) of Mg alloys, *Surf. Coat. Technol.*, 369(2019), p. 142.

[19] X.P. Lu, C. Blawert, K.U. Kainer, and M.L. Zheludkevich, Investigation of the formation mechanisms of plasma electrolytic oxidation coatings on Mg alloy AM50 using particles, *Electrochim. Acta*, 196(2016), p. 680.

[20] C. Ma, D. Wang, J.Y. Liu, N. Peng, W. Shang, and Y.Q. Wen, Preparation and property of self-sealed plasma electrolytic oxide coating on magnesium alloy, *Int. J. Miner. Metall. Mater.*, 30(2023), No. 5, p. 959.

[21] H.P. Han, R.Q. Wang, Y.K. Wu, *et al.*, An investigation of plasma electrolytic oxidation coatings on crevice surface of AZ31 magnesium alloy, *J. Alloys Compd.*, 811(2019), art. No. 152010.

[22] C.C. Liu, T. Xu, Q.Y. Shao, *et al.*, Effects of beta phase on the growth behavior of plasma electrolytic oxidation coating formed on magnesium alloys, *J. Alloys Compd.*, 784(2019), p. 414.

[23] X.Y. Wang, P.F. Ju, X.P. Lu, Y. Chen, and F.H. Wang, Influence of Cr_2O_3 particles on corrosion, mechanical and thermal control properties of green PEO coatings on Mg alloy, *Ceram. Int.*, 48(2022), No. 3, p. 3615.

[24] A. Ghanbari, A. Bordbar-Khiabani, F. Warchomicka, C. Sommitsch, B. Yarmand, and A. Zamanian, PEO/Polymer hybrid coatings on magnesium alloy to improve biodegradation and biocompatibility properties, *Surf. Interfaces*, 36(2023), art. No. 102495.

[25] N. Li, N. Ling, H.Y. Fan, L. Wang, and J.L. Zhang, Self-healing and superhydrophobic dual-function composite coating for active protection of magnesium alloys, *Surf. Coat. Technol.*, 454(2023), art. No. 129146.

[26] K. Qian, W.Z. Li, X.P. Lu, *et al.*, Effect of phosphate-based sealing treatment on the corrosion performance of a PEO coated AZ91D Mg alloy, *J. Magnesium Alloys*, 8(2020), No. 4, p. 1328.

[27] B. Mingo, R. Arrabal, M. Mohedano, *et al.*, Influence of sealing post-treatments on the corrosion resistance of PEO coated AZ91 magnesium alloy, *Appl. Surf. Sci.*, 433(2018), p. 653.

[28] M. Mohedano, C. Blawert, and M.L. Zheludkevich, Cerium-based sealing of PEO coated AM50 magnesium alloy, *Surf.*

[29] N.V. Phuong, B.R. Fazal, and S. Moon, Cerium- and phosphate-based sealing treatments of PEO coated AZ31 Mg alloy, *Surf. Coat. Technol.*, 309(2017), p. 86.

[30] Q.Q. Chen, X.P. Lu, M. Serdechnova, *et al.*, Formation of self-healing PEO coatings on AM50 Mg by *in situ* incorporation of zeolite micro-container, *Corros. Sci.*, 209(2022), art. No. 110785.

[31] J.B. Meng, H.M. Li, X.J. Dong, *et al.*, Corrosion protection of NiTi alloy via micro-arc oxidation doped with ZnO nanoparticles and polyacrylamide sol–gel sealing, *J. Mater. Sci.*, 58(2023), p. 13816.

[32] S. Moon, Corrosion behavior of PEO-treated AZ31 Mg alloy in chloride solution, *J. Solid State Electrochem.*, 18(2014), p. 341.

[33] L. Pezzato, R. Babbolin, P. Cerchier, *et al.*, Sealing of PEO coated AZ91 magnesium alloy using solutions containing neodymium, *Corros. Sci.*, 173(2020), art. No. 108741.

[34] M. Mohedano, P. Pérez, E. Matykina, B. Pillado, G. Garcés, and R. Arrabal, PEO coating with Ce-sealing for corrosion protection of LPSO Mg–Y–Zn alloy, *Surf. Coat. Technol.*, 383(2020), art. No. 125253.

[35] M.A. Abd El-Ghaffar, N.A. Abdelwahab, A.M. Fekry, M.A. Sanad, M.W. Sabaa, and S.M.A. Soliman, Polyester-epoxy resin/conducting polymer/barium sulfate hybrid composite as a smart eco-friendly anti-corrosive powder coating, *Prog. Org. Coat.*, 144(2020), art. No. 105664.

[36] G. Senthilkumar, G.S. Kaliaraj, P. Vignesh, R.S. Vishwak, T.N. Joy, and J. Hemanandh, Hydroxyapatite–barium/strontium titanate composite coatings for better mechanical, corrosion and biological performance, *Mater. Today Proc.*, 44(2021), p. 3618.

[37] F. Liu, D.Y. Shan, E.H. Han, and C.S. Liu, Barium phosphate conversion coating on die-cast AZ91D magnesium alloy, *Trans. Nonferrous Met. Soc. China*, 18(2008), No. S1, p. s344.

[38] Y.G. Chen, B.L. Luan, G.L. Song, Q. Yang, D.M. Kingston, and F. Bensebaa, An investigation of new barium phosphate chemical conversion coating on AZ31 magnesium alloy, *Surf. Coat. Technol.*, 210(2012), p. 156.

[39] P.X. Wu, Y.P. Dai, H. Long, *et al.*, Characterization of organo-montmorillonites and comparison for Sr(II) removal: Equilibrium and kinetic studies, *Chem. Eng. J.*, 191(2012), p. 288.

[40] T.D. Pham, T.T. Tran, V.A. Le, T.T. Pham, T.H. Dao, and T.S. Le, Adsorption characteristics of molecular oxytetracycline onto alumina particles: The role of surface modification with an anionic surfactant, *J. Mol. Liq.*, 287(2019), art. No. 110900.

[41] C. Bai, M. Guo, Z. Liu, Z.J. Wu, and Q. Li, A novel method for removal of boron from aqueous solution using sodium dodecyl benzene sulfonate and D-mannitol as the collector, *Desalination*, 431(2018), p. 47.

[42] L.Y. Xu, X.J. Fu, H.J. Su, H.L. Sun, R.C. Li, and Y. Wan, Corrosion and tribocorrosion protection of AZ31B Mg alloy by a hydrothermally treated PEO/chitosan composite coating, *Prog. Org. Coat.*, 170(2022), art. No. 107002.

[43] B. Vaghefinazari, S.V. Lamaka, C. Blawert, *et al.*, Exploring the corrosion inhibition mechanism of 8-hydroxyquinoline for a PEO-coated magnesium alloy, *Corros. Sci.*, 203(2022), art. No. 110344.

[44] Y. Chen, X.P. Lu, S.V. Lamaka, *et al.*, Active protection of Mg alloy by composite PEO coating loaded with corrosion inhibitors, *Appl. Surf. Sci.*, 504(2020), art. No. 144462.

[45] D.B. Huang, J.Y. Hu, G.L. Song, and X.P. Guo, Inhibition effect of inorganic and organic inhibitors on the corrosion of Mg–10Gd–3Y–0.5Zr alloy in an ethylene glycol solution at ambient and elevated temperatures, *Electrochim. Acta*, 56(2011), No. 27, p. 10166.

[46] Y.K. Zhu, M. Free, R. Woollam, and W. Durnie, A review of surfactants as corrosion inhibitors and associated modeling, *Prog. Mater. Sci.*, 90(2017), p. 159.

[47] A. Frignani, V. Grassi, F. Zanotto, and F. Zucchi, Inhibition of AZ31 Mg alloy corrosion by anionic surfactants, *Corros. Sci.*, 63(2012), p. 29.

[48] Y. Li, X.P. Lu, D. Mei, T. Zhang, and F.H. Wang, Passivation of corrosion product layer on AM50 Mg by corrosion inhibitor, *J. Magnesium Alloys*, 10(2022), No. 9, p. 2563.

[49] C. Liu, X.P. Lu, Y. Li, Q.Q. Chen, T. Zhang, and F.H. Wang, Influence of post-treatment process on corrosion and wear properties of PEO coatings on AM50 Mg alloy, *J. Alloys Compd.*, 870(2021), art. No. 159462.

[50] T. Bayram, S. Bucak, and D. Ozturk, BR13 dye removal using sodium dodecyl sulfate modified montmorillonite: Equilibrium, thermodynamic, kinetic and reusability studies, *Chem. Eng. Process. Process. Intensif.*, 158(2020), art. No. 108186.

[51] C.H. Xu, D.M. Wang, H.T. Wang, *et al*., Experimental investigation of coal dust wetting ability of anionic surfactants with different structures, *Process. Saf. Environ. Prot.*, 121(2019), p. 69.

[52] J.G. Speight, *Lange's Handbook of Chemistry*, McGraw-Hill Education, New York, 2005.

[53] H.Y. Wang, Y.L. Song, X.G. Chen, G.D. Tong, and L.Y. Zhang, Microstructure and corrosion behavior of PEO-LDHs-SDS superhydrophobic composite film on magnesium alloy, *Corros. Sci.*, 208(2022), art. No. 110699.

[54] S.I. Omonmhenle and I.J. Shannon, Synthesis and characterisation of surfactant enhanced Mg–Al hydrotalcite-like compounds as potential 2-chlorophenol scavengers, *Appl. Clay Sci.*, 127(2016), p. 88